

Five parameters are all you need (in Λ CDM)

Paulo Montero-Camacho^{*1}, Yin Li⁺¹, and Miles Cranmer²

¹*Department of Mathematics and Theory, Peng Cheng Laboratory,
Shenzhen, Guangdong, China*

²*Data Intensive Science, University of Cambridge, Cambridge, UK*

Abstract The standard cosmological model, with its six independent parameters, successfully describes our observable Universe. One of these parameters, the optical depth to reionization τ_{reio} , represents the scatterings that Cosmic Microwave Background (CMB) photons will experience after decoupling from the primordial plasma as the intergalactic medium transitions from neutral to ionized. τ_{reio} depends on the neutral hydrogen fraction x_{HI} , which, in turn, should theoretically depend on cosmology. We present a novel method to establish the missing link between cosmology and reionization timeline using symbolic regression. We discover the timeline has a universal shape well described by the Gompertz mortality law, applicable to any cosmology within our simulated data. Unlike the conventional tanh prescription, our model is asymmetric in time and a good fit to astrophysical constraints on x_{HI} . By combining CMB with astrophysical data and marginalizing over astrophysics, we treat τ_{reio} as a derived parameter, tightening its constraint to $< 3\%$. This approach reduces the error on the amplitude of the primordial fluctuations by a factor of 2.3 compared to Planck's PR3 constraint and provides a commanding constraint on the ionization efficiency $\zeta_{\text{UV}} = 26.9^{+2.1}_{-2.5}$. We expect further improvements in the near term as reionization constraints increase and our understanding of reionization advances.

^{*}pmontero@pcl.ac.cn, with equal contribution

[†]eelregit@gmail.com, with equal contribution

The Λ CDM cosmological model has proven extremely effective in predicting the evolution of our Universe, relying on only six parameters¹. In particular, it explains the transition from a predominantly neutral state in the early stages to the familiar ionized intergalactic medium (IGM) observed in our relatively nearby surroundings. This transition is known as cosmic reionization. Despite a comprehensive understanding of the astrophysical principles governing this transition, uncertainties persist regarding its precise timeline². The advent of the James Webb Space Telescope (JWST)³ represents a pivotal moment, substantially bolstering our ability to directly constrain the evolution of the neutral hydrogen fraction x_{HI} . This progress is being driven by JWST's enhanced detection capabilities, enabling the observation of high-redshift quasars⁴ and high-redshift galaxies^{5,6,7,8}.

Reionization leads to scattering of Cosmic Microwave Background (CMB) photons by free electrons, disrupting the CMB angular power spectra C_ℓ . This scattering suppresses the signal at scales smaller than the Hubble scale at reionization (approximately $\ell > 10$)⁹ due to the optical depth τ_{reio} . Additionally, it introduces a new signal in the polarization of CMB photons at large angular scales¹, that is $\propto \tau_{\text{reio}}$ in C_ℓ^{TE} , the cross-correlation of the E -mode polarization with the temperature (intensity), and is $\propto \tau_{\text{reio}}^2$ in C_ℓ^{EE} , the E -mode polarization angular auto power spectrum. Consequently, heightened sensitivity to CMB polarization becomes crucial for mitigating the degeneracy between τ_{reio} and other cosmological parameters, particularly A_s , the amplitude of the primordial scalar power spectrum, and r , the ratio of tensor-to-scalar modes¹⁰.

Low- ℓ polarization data is crucial to determine τ_{reio} ; however, the measurement of such a weak signal ($\sim 10^{-2} \mu\text{K}^2$) demands superb systematic and foreground control⁹. Furthermore, anomalous measurements in C_ℓ^{TE} at low multipoles¹ could indicate concerns to the cosmological interpretations at these angular scales. Ultimately, this challenging measurement may require adopting a comprehensive Bayesian framework to jointly consider cosmology, astrophysics, and instrument systematics¹¹. **Figure 1** illustrates current representative constraints on τ_{reio} .

Given the challenges posed by τ_{reio} in CMB analyses and the anticipated advancements in constraining the reionization timeline^{19,20}, now is an opportune moment to reassess its role. Theoretically, cosmic reionization is uniquely determined by cosmology, i.e. $x_{\text{HI}}(z)$ is fully determined by the other five cosmological parameters. However, incomplete understanding of reionization obscures this mapping, necessitating the additional empirical parameter τ_{reio} in CMB analyses. Since the inclusion of τ_{reio} became a standard practice, our understanding of the astrophysical processes governing reionization has significantly improved^{21,22,23,24} and ongoing and forthcoming observations promise to reduce inherent modeling uncertainties.

Motivated by these developments, we use symbolic regression (SR)²⁵ to construct a mapping between cosmology, astrophysics, and reionization timeline, aiming to demote τ_{reio} from an independent to a derived cosmological parame-

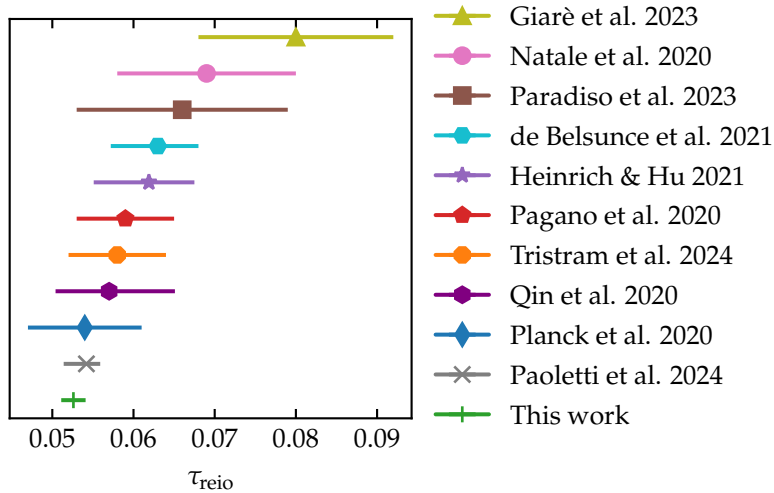


Figure 1: Current constraints on the optical depth to reionization (τ_{reio}) from Cosmic Microwave Background (CMB) data. The error bars indicate the 1σ uncertainties. Various analyses may employ distinct data sets or vary in the parameters considered. For instance, the inclusion of astrophysical data^{12,13} (cross and purple hexagon), WMAP data^{10,11} (circle and square), or ACT in combination with other external data sets¹⁴ (triangle), expanded sky coverage¹¹ (square), incorporation of high- ℓ data^{15,16,14,17} (pentagon, diamond, star, triangle, and octagon), joint low- ℓ TT and EE analysis¹⁸ (cyan hexagon), marginalization over small set of strongly correlated parameters¹⁰ (circle), and the implementation of an end-to-end Bayesian framework that marginalizes over astrophysics and instrumental systematics¹¹ (square).

ter and simultaneously tightening constraints in cosmological and astrophysical parameters. This mapping can also shed light on reionization astrophysics and aid ongoing efforts in parametrizing reionization models^{26,27,13} by including the cosmological dependence of x_{HI} .

Here, we present a universality in the neutral hydrogen time evolution related via a power-law transform, and derive through SR the dependence of power-law parameters on cosmology and astrophysics from simulated 21cmFAST^{28,23} reionization histories. We integrate this universally shaped reionization timeline into CLASS²⁹, a popular Boltzmann solver for CMB analyses. We then evaluate the modified CLASS alongside Cobaya³⁰, a speed-aware sampler^{31,32}, showcasing its ability to recover parameter constraints from CMB data, including ‘TTTEEE’ + lensing likelihoods^{33,34} (see Figure 9). Finally, combining CMB and astrophysical data, we marginalize over reionization astrophysics to compute τ_{reio} as a derived parameter using SR, quantifying the gains compared to sampling over τ_{reio} utilizing the conventional tanh model³⁵. We summarize our strategy in Figure 2.

We construct the universal x_{HI} shape using 256 Sobol samples of 21cmFAST simulations, varying 5 cosmological parameters and the astrophysical ionizing efficiency ζ_{UV} . The latter modulates the timing of reionization by regulating the abundance of photons that escape into the IGM (see Simulations and Figure 5 in

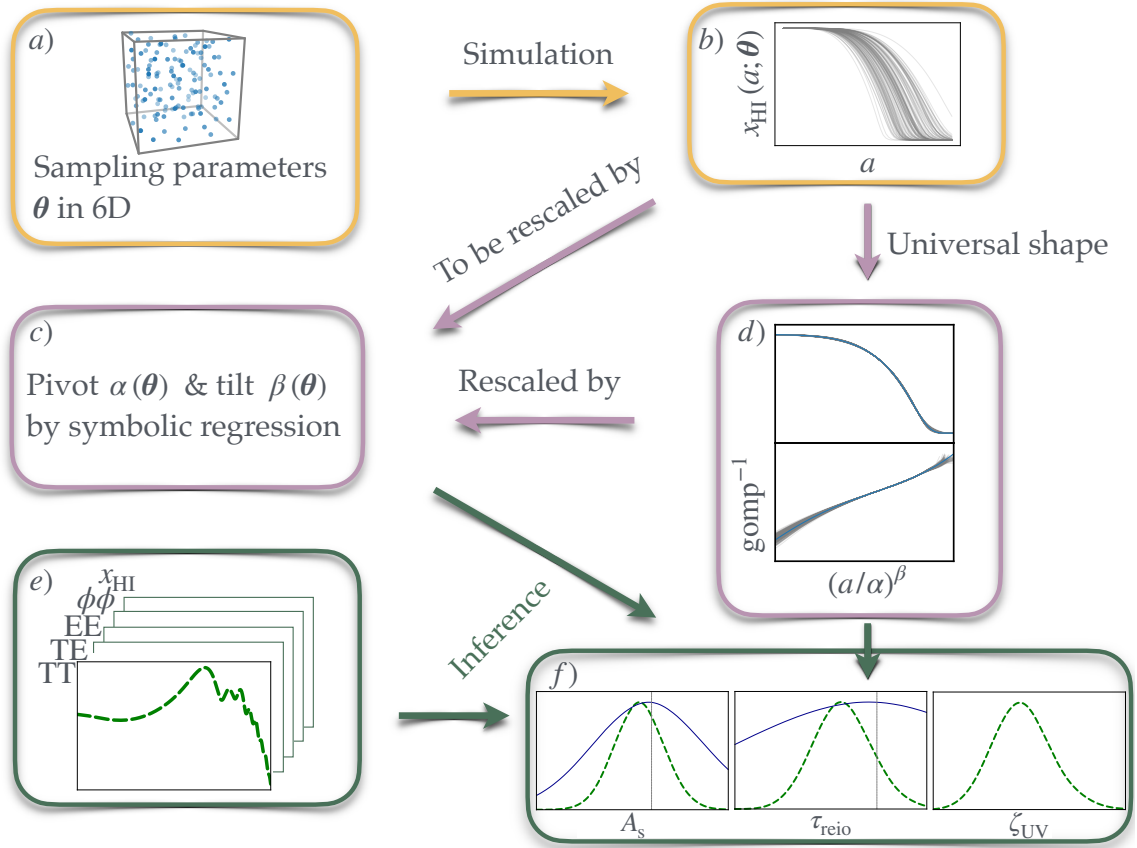


Figure 2: Strategy to demote τ_{reio} to derived parameter. *a)* Sobol sampling of θ comprising 5 cosmological and 1 astrophysical parameters (see Figure 5 in Extended Data). *b)* Simulated x_{HI} timelines as a function of θ and scale factor a . *c)* With symbolic regression, we optimize the mapping from θ to the rescaling parameters that bring the universality. *d)* We model the universal shape (upper panel) as a composition of the Gompertz function and a low-degree polynomial (lower panel). *e)* Planck CMB data and x_{HI} data we analyze. *f)* We infer the parameter constraints using Monte Carlo Markov Chain (MCMC).

the Extended Data). All $x_{HI}(a)$ profiles share the same shape, with differences between scenarios being mere translations and rescalings in logarithmic scale factor $\ln a$. Reionization causes x_{HI} to reduce from near 1 to effectively 0 via a sigmoid transition. The standard tanh function is symmetric in nature and not flexible enough to provide the early start and rapid completion suggested by reionization simulations^{26,36} and favored by astrophysical data (see Figure 4). In contrast, the SR-inspired Gompertz curve, an asymmetric sigmoid function often used to analyze age-dependent human mortality³⁷, proves a good model for the survival of neutral hydrogen too. Its expected accelerated increase in mortality with age resembles the expectation for the percolation of ionized hydrogen bubbles during the end stages of reionization.

One way to uncover the universality is to view each x_{HI} scenario as a cumulative probability distribution (CDF) in $-\ln a$. With this insight, we can translate and rescale each timeline using the mean and variance of its corresponding probability

density function (PDF), i.e. $-dx_{\text{HI}}/d \ln a$, and discover the existence of a universal shape followed by all scenarios. Therefore, cosmology and ζ_{UV} only impacts the translation and rescaling parameters of each timeline, not its shape.

However, with the PDF trick, some x_{HI} 's can deviate artificially from universality, due to their incomplete reionization given our broad range of simulated scenarios. To address this, we adopt a better approach to jointly fit the global shape and the 2 individual parameters of each x_{HI} . Our shape model constitutes the Gompertz function composed with a 5th-degree polynomial, in the translated-and-rescaled time $\ln \tilde{a} \equiv \beta(\ln a - \ln \alpha)$. And we are free to set the polynomial constant to 0 and its linear coefficient to 1 by utilizing their respective degeneracy with $\ln \alpha$ and β .

The complete model parametrizes the HI evolution as follows (also see [Figure 6](#) and [Shape universality and modeling](#) in the Extended Data):

$$x_{\text{HI}}(\tilde{a}) = \text{gomp}(P_5(\tilde{a})) \equiv \exp[-\exp(P_5(\tilde{a}))], \quad (1)$$

$$P_5(\tilde{a}) = \sum_{m=0}^5 c_m \ln^m \tilde{a}, \quad (2)$$

$$c = \{0, 1, 0.1130, 0.02600, 0.0005491, -0.00006518\},$$

$$\tilde{a}(a; \boldsymbol{\theta}) = \left[\frac{a}{\alpha(\boldsymbol{\theta})} \right]^{\beta(\boldsymbol{\theta})}, \quad (3)$$

where $\boldsymbol{\theta}$ denotes 6 astrophysical and cosmological parameters, $\alpha(\boldsymbol{\theta})$ is the power-law pivot (or logarithmic translation), and $\beta(\boldsymbol{\theta})$ is the rescaling tilt. Their parameter dependences stem from 21cmFAST's modeling of reionization astrophysics. Also see [Helium reionization](#) for specifics on implementing HeI and HeII reionization.

Before fully leveraging our methodology to extract the parameter dependence in the rescaling of [Eq. \(1\)](#) and relaxing the need for τ_{reio} in CMB analyses, we first implement the Gompertz shape with independent τ_{reio} in CLASS and confirm its agreement with the conventional tanh model (gomp and tanh in [Table 1](#)). Using Planck PR3 likelihoods 'TTTEEE'³³ and CMB lensing³⁴, we sample typical cosmological parameters with Cobaya³⁰, including τ_{reio} . Given a proposal for τ_{reio} , we determine the corresponding reionization timeline using bisection by varying $\ln \alpha$ for gomp while fixing β to its mean value, meanwhile for tanh, the reionization midpoint z_{re} is the tuning parameter. The sampler runs until the Gelman-Rubin statistic³⁸ satisfies $R - 1 < 0.01$ for the variance in parameter means from different chains. We repeat this for tanh and verify the agreement between the two models.

[Figure 9](#) and [Table 1](#) in the Extended Data summarize this validation experiment. The only notable differences in inferred parameters are in z_{re} . The gomp scenario suggests a more delayed reionization by over 1σ , with $z_{\text{re}} = 6.76 \pm 0.67$ compared to 7.67 ± 0.75 for tanh, in alignment with recent high- z quasar observations³⁹. All other cosmological parameters are in good agreement with Planck's results¹, with differences $\lesssim 0.5\%$.

Having demonstrated that the universally shaped reionization can reproduce standard CMB analyses, we move to establish the connection between the universal

shape for x_{HI} and the rescaling of a given reionization scenario. We refer to this model as `gomp + SRFull`. This rescaling naturally depends on cosmology and astrophysics. For example, a larger matter density Ω_{m} results in deeper potential wells, accelerating structure formation and increasing the number of ultraviolet photons driving the reionization process. We employ PySR, an SR package, to establish the parameter dependences of the rescaling in Eq. (3).

While PySR initially guided us towards the Gompertz curve when directly regressing x_{HI} , the final analysis only uses it to regress the pivot and tilt instead. We fit their values jointly with the polynomial coefficients as described above, and feed them as labels to the genetic algorithm to find the best analytic expression (see [Symbolic regression](#) in Extended Data for our definition of *best*). Using PySR we derived the following mapping

$$\ln \alpha(\boldsymbol{\theta}) = \left(\frac{\Omega_{\text{b}}}{\Omega_{\text{m}}} \right)^h - (\sigma_8 - 0.04835)(n_s + 0.3558 \ln(0.1123\zeta_{\text{UV}})) - \Omega_{\text{m}} - n_s, \quad (4)$$

$$\beta(\boldsymbol{\theta}) = \left(\frac{0.005660\Omega_{\text{m}}}{0.6015} - \ln(\zeta_{\text{UV}} - (\Omega_{\text{m}} + n_s h)^{15.05}) + h \right) \ln \Omega_{\text{b}} + \frac{h}{\sigma_8}, \quad (5)$$

where n_s , h , Ω_{b} , and Ω_{m} are the tilt of the primordial power spectrum, dimensionless Hubble constant, and present baryon and matter density fractions, respectively. σ_8 is the present linear rms relative density fluctuation in a sphere of radius $8 h^{-1}\text{Mpc}$.

Eqs. (3) to (5) are analytic expressions and thus interpretable. For example, higher values of Ω_{m} , σ_8 , and ζ_{UV} hasten reionization by enhancing structure formation and increasing the abundance of ionizing photons. Similarly, larger n_s primarily expedites reionization by boosting power on small scales, leading to more ionizing sources and earlier completion¹⁹. Keep in mind that our 21cmFAST simulations assume that faint galaxies are the primary drivers of reionization. Surprisingly, Eqs. (4) and (5) suggests that higher Ω_{b} delays reionization, likely due to more HI in the intergalactic medium requiring additional ionizing photons. The ratio $\Omega_{\text{b}}/\Omega_{\text{m}}$ in α supports this view. Moreover, increasing h slightly delays reionization, consistent with an increase in physical baryon density and the expectation that galaxies and ionizing photons will be more spread out.

We note that within the prior range of our 21cmFAST simulations (see [Simulations](#)) and their corresponding astrophysics of reionization, the mapping derived from SR is not unique. Additional details and results using an alternative mapping – SRHalf – are presented in [Alternative mapping](#) of the Extended Data. Nonetheless, our results are robust and independent of the choice of mapping.

We implement Eqs. (4) and (5) in our Gompertz CLASS, which given the cosmological and astrophysical parameters, determines the pivot and tilt values, and consequently the reionization history, τ_{reio} , and CMB angular power spectra. This `gomp + SRFull` model eliminates the need to sample over τ_{reio} (or z_{re}), requiring only five cosmological parameters and ζ_{UV} . Moreover, thanks to SR, the model

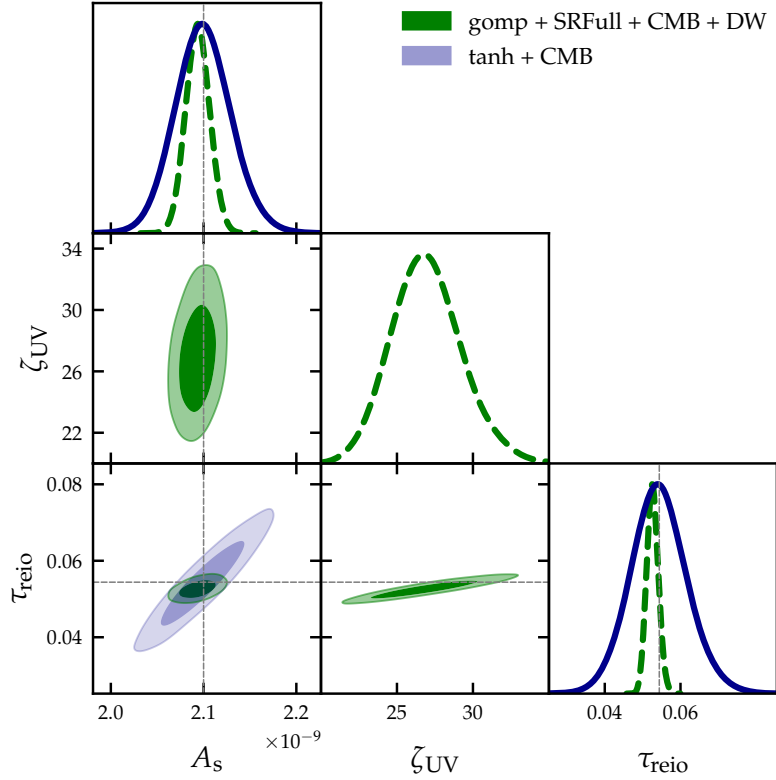


Figure 3: Analysis of CMB and astrophysical data with reionization as a function of cosmology and astrophysics. The green contours represent our results using the Gompertz reionization model with Eqs. (4) and (5), which eliminates the need to sample over any conventional reionization parameter and uses quasar damping wing data on x_{HI} to constrain and marginalize over reionization astrophysics. The blue contours correspond to the results obtained using the conventional tanh model, while the relevant Planck constraints¹ are depicted with gray lines for reference. The tanh model performs poorly in fitting astrophysical data; thus, combining tanh with astrophysical data is ill-advised.

can constrain ζ_{UV} using CMB and astrophysical data directly, a link that was not utilized in previous efforts⁴⁰. The advantage of sampling over ζ_{UV} instead of τ_{reio} is that powerful astrophysical constraints on x_{HI} can be used to marginalize over ζ_{UV} . We use Cobaya to re-analyze the same CMB data and include astrophysical data (see **Astrophysical data** of the Extended Data) to effectively constrain and marginalize over ζ_{UV} .

Figure 3 underscores the impact of our universally-shaped Gompertz reionization model, tightening the optical depth constraint to $< 3\%$ compared to $> 10\%$ with the tanh prescription. Furthermore, the constraint on A_s improves dramatically since the TT data is no longer significantly hampered by the degeneracy between A_s and τ_{reio} . The error on A_s decreases by an impressive factor of 2.3 compared to Planck’s results¹. Overall, we recover tighter constraints across the board compared to Planck. Notably, combining SR with CMB and astrophysical data, specifically quasar damping wing (DW) data, yields a highly competitive constraint on $\zeta_{\text{UV}} = 26.9^{+2.1}_{-2.5}$, a commanding improvement over previous constraints (e.g.

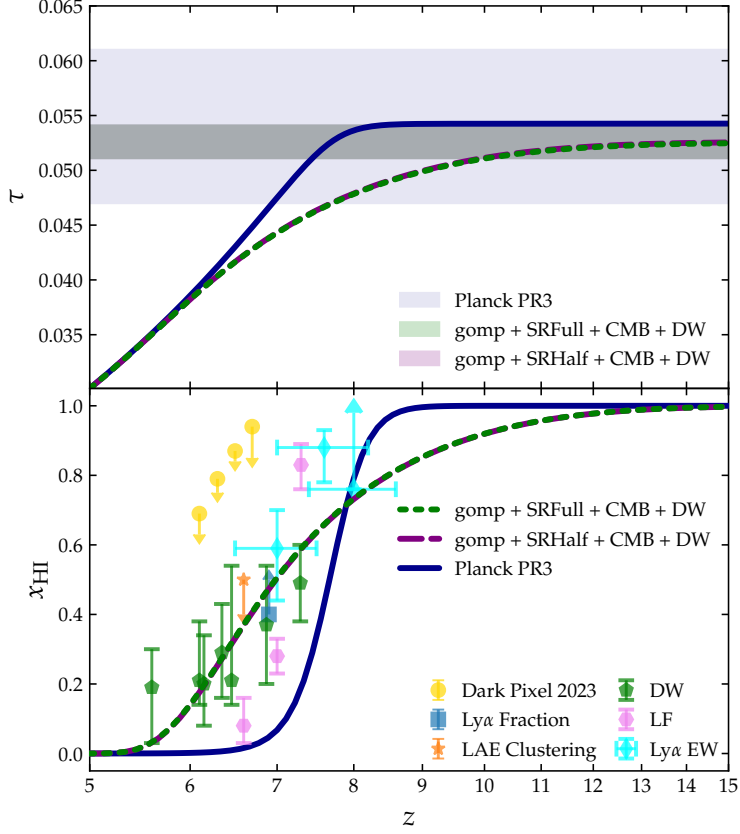


Figure 4: Optical depth evolution $\tau(z)$ and reionization history $x_{\text{HI}}(z)$. Our best-fit gomp + SRFull model (green dotted line) of Planck CMB data + quasar damping wing (DW) data is asymmetric and differs significantly from that of the symmetric tanh model (blue solid line). Note z is shown in logarithmic scale of a^{-1} . We also include an alternative mapping from physical parameters to Gompertz timeline – gomp + SRHalf – in the purple dashed line (see [Alternative mapping](#)). The shaded regions in the upper panel correspond to the inferred range in τ_{reio} from analyzing Planck PR3 data. Additionally, the lower panel includes observational constraints from high-redshift quasars and galaxies (see [Astrophysical data](#)).

$\zeta_{\text{UV}} = 28^{+52}_{-18}$ ⁴⁰. See [MCMC inference](#), [Figure 8](#) and [Table 1](#) in the Extended Data for details.

Our results suggest that Planck data favors a delayed reionization compared to other CMB-based constraints (in a χ^2 -sense). Our best-fit cosmological parameters indicate a midpoint of $z_{\text{re}} = 6.98$ and a duration of $\Delta z \equiv z(x_{\text{HI}} = 0.05) - z(x_{\text{HI}} = 0.95) \approx 560$ Myr, consistent with our previous constraint without SR. While our results align with late reionization observations, the difference from tanh is within 1σ . The duration of reionization, though better suited to observational constraints compared to tanh, might still be considered somewhat rapid in the context of late reionization scenarios⁴¹. [Figure 4](#) illustrates the reionization timeline derived from our best-fit values, in contrast with the poor fit of symmetric tanh to the astrophysical data.

Our findings for the timeline of reionization align with late reionization scenarios, which are supported by high- z Lyman- α observations^{39,41}. However, recent discoveries by JWST indicate the presence of massive, bright galaxies at early redshifts $z \sim 10$ ^{5,6,7}. The presence of these early galaxies suggests a potential preference for brighter galaxies to drive reionization, a role that in our 21cmFAST simulations was attributed to a population of faint galaxies.

We note that our results assume a flat Universe. Relaxing this assumption requires adding an extra parameter to the functional form of τ ⁴². Furthermore, our results are influenced by the semi-numerical prescription employed by 21cmFAST to ionize the IGM, which, while efficient and swift, could bias our findings. Moreover, our exploration within the astrophysical framework of 21cmFAST has been limited to varying the ionization efficiency (see [Simulations](#) in the Extended Data). Therefore, a more comprehensive exploration is warranted to ensure, for instance, that our findings for α and β will not bias cosmological analyses when incorporating additional astrophysical parameters, such as the minimum halo mass that host ionizing sources. Additionally, a valuable exercise to refine the inherent relationship between cosmological parameters and reionization history would involve using more realistic, albeit slower, reionization models. One such option is to use the THESAN simulations²², which are hydrodynamical simulations incorporating radiative transfer.

Throughout this work we considered only DW for astrophysical data, but including current luminosity function constraints can already halve the error on τ_{reio} . Hence, as reionization constraints improve, we anticipate substantial cosmological gains with our framework.

Methodology

Simulations

To establish the universality of our proposed Gompertz model for the neutral hydrogen reionization and its relationship with the cosmological parameters, we conducted 256 21cmFASTv3 simulations to generate the corresponding $x_{\text{HI}}(z; \theta)$ profiles. Our parameter space include $\theta = \{\sigma_8, n_s, h, \Omega_b, \Omega_m, \zeta_{\text{UV}}\}$, comprising five cosmological and one astrophysical parameters. The selection of σ_8 instead of A_s is imposed by the input requirements of 21cmFAST¹. We first use a scrambled Sobol sequence^{44,45} of length 128 to sample quasi-uniformly within the following θ -ranges:

$$\begin{aligned} \sigma_8 &\in (0.74, 0.90), & n_s &\in (0.92, 1.00), & h &\in (0.61, 0.73), \\ \Omega_b &\in (0.04, 0.06), & \Omega_m &\in (0.24, 0.40), & \zeta_{\text{UV}} &\in (20, 35). \end{aligned} \quad (6)$$

¹Alternatively, one could use 21cmFirstCLASS⁴³ to avoid σ_8 .

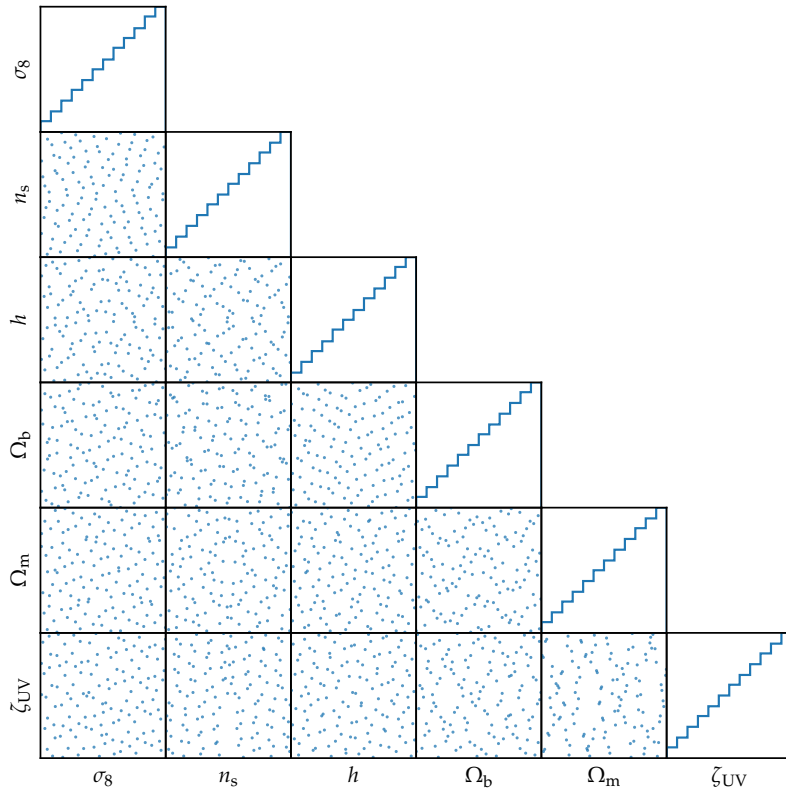


Figure 5: Sobol design for our x_{HI} edge and core samples, in 6D parameter space of σ_8 , n_s , h , Ω_b , Ω_m , and ζ_{UV} . Each of the 128 points in the lower triangular panels corresponds to the 2D projection of one core and one edge 21cmFAST runs, while the diagonal panels show the 1D cumulative histograms for each parameter. These 1D and 2D projections demonstrate the uniformity of our sampling of the parameter space within the edge prior range of Eq. (6), as well as in the core area surrounding the Planck PR3 constraint.

Their 1D and 2D projections in Figure 5 illustrate the sample uniformity in parameter space. Because most of the 6D hypercube volume lies near its surface, we name the above 128 simulations the *edge* samples and let the other 128 simulations sample its *core* within the 5σ range of Planck PR3 constraint¹, reusing the same Sobol design in Figure 5. This helps to improve the accuracy of symbolic regression where the final posterior mass are expected to lie.

Our 21cmFAST simulations have a 300 comoving Mpc box size and 768^3 (256^3) cells for the matter (HI) field. We maintain most options in their default values and extract the neutral hydrogen fraction using `lightcone.global_xH`.

The ionization efficiency ζ_{UV} governs the ability of ultraviolet photons to escape their parent galaxies and ionize the IGM. An increase in ζ_{UV} leads to an earlier completion of HI reionization. Due to significant uncertainties surrounding ζ_{UV} , we opted to use a constant value in each simulation. Note that this choice was made for simplicity, and a more realistic assumption could be that ζ_{UV} is a function of halo mass⁴⁶ or redshift, which we will investigate in future work.

Helium reionization

The early intergalactic medium is primarily composed by neutral hydrogen and helium. Neutral helium (HeI) loses its first electron at the same time as neutral hydrogen (HI) gets ionized⁴⁷. However, there is a second reionization that occurs around $z \sim 3$ where Helium (HeII) loses its remaining electron.

CMB photons will scatter off any free electrons, therefore both helium reionizations contribute to the Thomson optical depth to reionization τ_{reio} , although HeII ionization contribute relatively little in comparison to HI and HeI ionizations⁴⁸.

To include the impact of the first helium reionization in our Gompertz CLASS, we assume it follows that of HI as done in the tanh model, i.e. the free electron fraction x_e is given by

$$\begin{aligned} x_e &= \left(1 + \frac{n_{\text{He}}}{n_{\text{H}}} - x_e^{\text{rec}}\right) x_e^{\text{gomp}} + x_e^{\text{rec}} \\ &= \left(1 + \frac{Y_{\text{He}}}{C(1 - Y_{\text{He}})} - x_e^{\text{rec}}\right) x_e^{\text{gomp}} + x_e^{\text{rec}}, \end{aligned} \quad (7)$$

where $n_{\text{He}}/n_{\text{H}}$ is the helium to hydrogen number density ratio, $C \equiv m_{\text{He}}/m_{\text{H}} \approx 4$ is their mass ratio, Y_{He} is the helium mass fraction, x_e^{gomp} corresponds to the contribution of free electrons due to Eq. (1), and $x_e^{\text{rec}} \approx 10^{-4}$ is the leftover free electrons from after recombination.

Given the relatively small impact of the HeII reionization on τ_{reio} , the current uncertainties regarding its timeline, and the difficulty involved with its accurate modeling^{49,50}, we opt to follow the conventional approach and include the second Helium reionization using the tanh model

$$x_e^{\text{Tot}} = x_e + \frac{Y_{\text{He}}}{2C(1 - Y_{\text{He}})} \left(\tanh \left(\frac{z_{\text{re}}^{\text{HeII}} - z}{\Delta z^{\text{HeII}}} \right) + 1 \right), \quad (8)$$

where $z_{\text{re}}^{\text{HeII}} = 3.5$ and $\Delta z^{\text{HeII}} = 0.5$ are the midpoint and duration of the second helium reionization, respectively. These choices are also the default values used by CLASS.

Shape universality and modeling

We discovered the universality in the shape of x_{HI} timelines before attempting to build analytic model for it. Because x_{HI} varies monotonically between 1 and 0, we can view it as a CDF and derive its PDF, with which we can weigh the logarithmic scale factor $\ln a$ to compute its mean and standard deviations. It was immediately obvious to us that the x_{HI} 's had a common shape to percent level, after translation by their means and rescaling by their standard deviations. However, given our broad parameter range in Eq. (6), some x_{HI} 's have not reached 0 by the end of simulations, resulting in imperfect transformations hurting the universality.

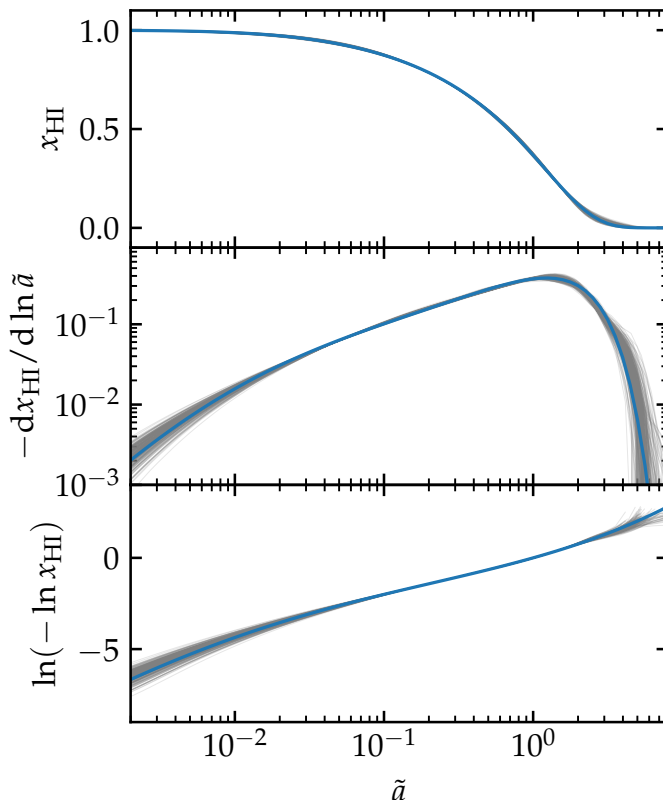


Figure 6: Universal shape of x_{HI} . (Top) 256 simulated x_{HI} timelines (thin light gray lines) exhibit universality, after power-law transformations $\tilde{a} = (a/\alpha)^\beta$. The blue curves in all panels show our fitted analytic shape model, a composition of the Gompertz curve with a 5th-degree polynomial in Eqs. (1) and (2). (Middle) Time derivative of x_{HI} , can be interpreted as a PDF if we view x_{HI} itself as the CDF. We first discovered the universality by translating and rescaling each x_{HI} using the mean and variance of its PDF, though now switch to the better approach that jointly fits the global shape and individual power-law parameters. We use the latter as target of symbolic regression. (Bottom) Timelines transformed by the inverse of Gompertz function, modeled in blue curve with a 5th-degree polynomial in Eq. (2).

To address this, we construct flexible models for the universal shape, and fit it jointly with individual transformation parameters of each x_{HI} timeline. We compose the Gompertz function gomp , defined in Eq. (1), with a low-degree polynomial P_m , where $m = 1, 3, 5, 7$ progressively. We fit the composed shape to minimize the mean squared error (MSE) in 256 x_{HI} 's and at 127 time points in each, and find the objective value improve with m but only marginally from P_5 to P_7 . Therefore, our final shape model is a composition of gomp and P_5 , (see the lower panel of Figure 6), and has 6 parameters to fit.

As for the transformation parameters, as in the PDF approach, we use an affine transformation $\ln \tilde{a} = \beta(\ln a - \ln \alpha)$, or equivalently a power law in Eq. (3). Because each x_{HI} has its own parameters of α and β , we have in total $518 = 6 + 2 \times 256$ parameters to determine in the joint fit. Figure 6 shows all 256 x_{HI} timelines and

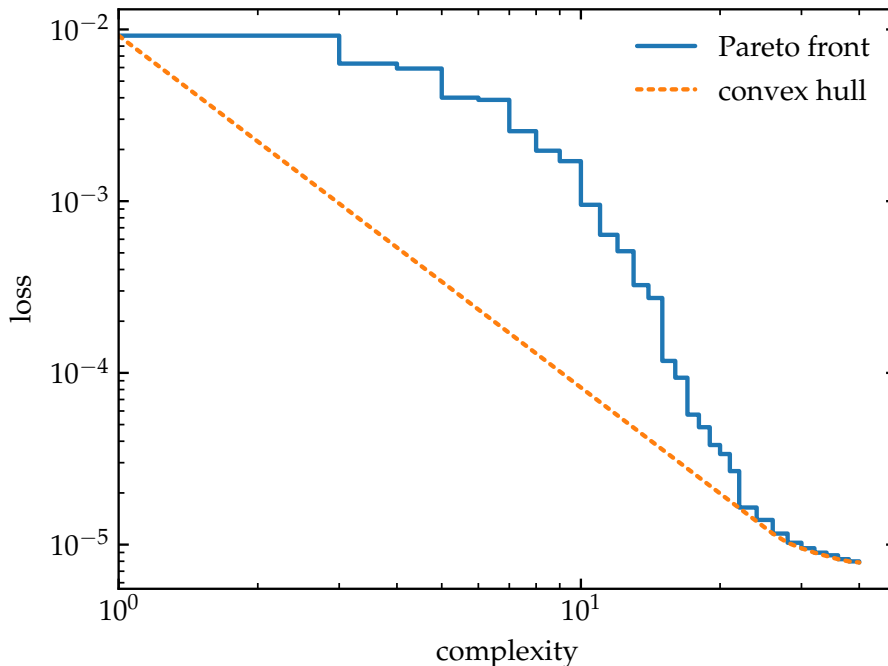


Figure 7: Pareto front for symbolic regression (blue solid steps) illustrates the trade-off between regression accuracy and expression complexity. We further add the lower convex hull to aid model selection: each segment of the orange dotted line represents a power-law trade-off in this log-log plot, and every model that touches the convex hull is more economic – in the sense of accuracy gain at cost of complexity – than the nearby models above the segments. As an example, here we show the results of $\ln \alpha(\theta)$, where the complexity 22 point gives Eq. (4).

their universality after transformations. We can then use the fitted α and β as the target for symbolic regression, to model their dependences on the independent cosmological and astrophysical parameters.

Symbolic regression

SR learns a model of data in the form of analytic expressions. Unlike traditional fittings that are restricted by their specific parameterization, SR searches in the vast function space of all expressions composed of specified operations, input variables, and free constants. It is NP-hard^{51,52} and typically need genetic or deep learning-based algorithms. In this work, we use the PySR package^{53,25} which performs SR optimizations using a multi-population genetic algorithm.

With PySR, we search for symbolic expressions that take the 6 parameters in Figure 5 as inputs and output $\ln \alpha$ or β , to minimize the MSE loss. Here, the search space is the set of expressions composed of 5 binary operators (+, -, ·, /, and power function) and 2 unary operators (exp and ln). Each expression naturally takes the form of a binary tree, and the total number of nodes is a measure of its complexity. We use 512 PySR populations each having 33 expressions, and optimize for 20000

iterations each with 10000 cycles.

More complex expressions tend to fit more accurately, a trade-off typically visualized by the Pareto front, as shown in [Figure 7](#). Better and more economic expressions can achieve a lower loss at moderate increase of complexity. To aid model selection, we use a heuristic that compares all expressions on the Pareto front globally, and only considers models that fare favorably in power-law trade-offs of the form

$$\text{loss}^{1-\gamma} \cdot \text{complexity}^\gamma = \text{const}, \quad \forall \gamma \in (0, 1). \quad (9)$$

All such expressions lie on the lower convex hull of the Pareto front, as illustrated in [Figure 7](#).

For the pivot $\ln \alpha$, we find complexity 22 is enough for the MSE loss to reach 1.6×10^{-5} (lower than sub-percent level error on average), so there is no need to use expressions more complex than that. For the tilt β , complexity 25, corresponds to a loss $\approx 1.2 \times 10^{-3}$ ($\lesssim 0.05\%$ error on average), while higher complexities can help but very slowly. Therefore, based on the economic heuristic, we choose expressions of complexity 22 and 25, for $\ln \alpha$ and β , respectively.

Our current selection for tilt and pivot could be a consequence of the astrophysical assumptions of reionization in 21cmFAST. A more complex simulation, such as one involving radiative transfer or different X-ray preheating⁵⁴, might reveal a different mapping between physical parameters and x_{HI} profiles.

Alternative mapping

The mapping between neutral hydrogen profiles and cosmology is not unique. This is because symbolic regression algorithms can be non-convergent. Moreover, the resulting symbolic expressions can depend on the data used for training, i.e. overfitting.

To investigate the impact of overfitting, we train an alternative mapping of reionization with cosmology using only half of the 21cmFAST x_{HI} profiles, which we refer as SRHalf. For the pivot and tilt, we obtain

$$\ln \alpha(\boldsymbol{\theta}) = \left(\frac{\Omega_{\text{b}}}{\Omega_{\text{m}}} \right)^{\Omega_{\text{m}}} - \ln^{0.5271} \left(h \left(\zeta_{\text{UV}} + \Omega_{\text{b}}^{-0.4982} \right)^{\sigma_8} \right) - n_{\text{s}}^{1.834}, \quad (10)$$

$$\beta(\boldsymbol{\theta}) = \left(\frac{\zeta_{\text{UV}} - \Omega_{\text{m}}^{-1.583}}{\Omega_{\text{b}} h} \right)^{0.3163}, \quad (11)$$

with a training loss (complexity) of 1.1×10^{-5} (22) and 3.7×10^{-3} (11), respectively. Overall, we obtain a relative root mean squared error of 0.9% when reproducing the simulated optical depths from the x_{HI} (edge + core) with SRHalf. Now we can test this on the other half of our x_{HI} sample and get a validation loss of 2.2×10^{-5} and 6.5×10^{-3} respectively, only slightly larger than the training loss on absolute scales, which implies that we are safe from overfitting, supported by consistency

of their MCMC results.

Unsurprisingly, Eqs. (10) and (11) recover the cosmological trends discovered with SRFull. Specifically, increasing ζ_{UV} , n_s , Ω_m , and σ_8 primarily leads to earlier reionization, while larger Ω_b delays it. The ratio of matter densities appears in the pivot expression again. Notably, the role of h generally shows the opposite trend in α . Furthermore, Eq. (11) excludes n_s and σ_8 because of our choice of complexity for SRHalf, which, despite having a larger loss, still achieves mean squared errors comparable to SRFull when reproducing the simulated data.

Replacing Eqs. (4) and (5) with Eqs. (10) and (11), we rerun the analysis following the same approach, and summarize the results using CMB jointly with astrophysical data in Table 1. Comparing these findings to our previous results, we observe strikingly similar values for all cosmological parameters. The consistency between our results using the full x_{HI} sample and those using only half of it indicates that our symbolic expression mappings perform robustly and are not biasing the parameter inferences.

Astrophysical data

The increasing number of direct constraints on the reionization timeline enhances CMB analyses. Figure 4 includes upper limits from dark pixel constraints² (high- z quasars), a lower bound from the Ly α emission fraction⁵⁵ (high- z galaxies), and an upper limit from the clustering of Ly α emitters⁵⁶ (high- z galaxies). It also presents constraints by Ly α equivalent width of Ly α emitters^{57,58,59} (high- z galaxies) and quasar damping wings^{60,61,62,63} (high- z quasars). Furthermore, it includes the indirect constraints on x_{HI} through the evolution of the galaxy Ly α luminosity function⁶⁴.

In this work, we supplement Planck CMB data with quasar damping wing (DW) constraints on x_{HI} (green pentagons in Figure 4), reflecting our confidence in their robustness. Future studies could include luminosity function (LF) constraints as more data becomes available, particularly since we find including them could already halve the error on τ_{reio} , and because more data will enhance our ability to constrain and marginalize over reionization astrophysics. We opt not to include the LF constraints on x_{HI} in this work as they are in slight tension with the DW data at the current stage (Figure 4).

MCMC inference

Our inference combines CMB with astrophysical data. Table 1 summarizes the results obtained by performing MCMC Bayesian inference with Cobaya for the models considered throughout this work. We also include the Planck results¹ for reference. In total, we run one Gompertz and one tanh reionization models with CMB data and two extra Gompertz models using SR and astrophysical data jointly

Table 1: Parameter constraints from Planck CMB and astrophysical (DW) data. Summary table of the constraints for representative parameters of the universal shape (Gompertz) and tanh reionization models. The constraints use CMB ‘TTTEEE’ + lensing information alone or jointly with quasar damping wing x_{HI} constraints. The results from Planck analysis¹ are included for comparison. The validation models are gomp and tanh, gomp does not include the cosmological and astrophysical dependences present in the timeline of reionization. In contrast, gomp + SRFull, and the alternative mapping gomp + SRHalf, both include the additional parameter dependences in the reionization timeline. The shaded cells highlight the parameters that are sampled over by MCMC for the different models. The numbers in parentheses give the marginalized 1σ uncertainty in the last two significant digits. We highlight the best constraints in boldface, with improvements by factors of 5 and 2.3 on τ_{reio} and A_s , respectively. We also highlight our extremely competitive ζ_{UV} constraint. The age of the Universe and H_0 are in unit of Gyr and km/s/Mpc, respectively, and $S_8 \equiv \sigma_8 \sqrt{\Omega_m}/0.3$ as usual.

| Parameter | CMB | | | CMB + DW | |
|----------------------|-------------------------|-------------|-------------|---|---|
| | Planck PR3 ¹ | tanh | gomp | gomp + SRFull | gomp + SRHalf |
| $10^9 A_s$ | 2.100(30) | 2.099(30) | 2.101(31) | 2.094(13) | 2.094(13) |
| n_s | 0.9649(42) | 0.9641(42) | 0.9640(42) | 0.9636(39) | 0.9637(39) |
| $\Omega_c h^2$ | 0.1200(12) | 0.1201(12) | 0.1200(12) | 0.1202(11) | 0.1202(11) |
| $\Omega_b h^2$ | 0.02237(15) | 0.02235(15) | 0.02235(15) | 0.02234(14) | 0.02234(14) |
| Ω_m | 0.3153(73) | 0.3157(76) | 0.3155(75) | 0.3166(69) | 0.3163(69) |
| $\Omega_m h^2$ | 0.1430(11) | 0.1430(11) | 0.1430(11) | 0.1432(10) | 0.1431(10) |
| Ω_Λ | 0.6847(73) | 0.6842(76) | 0.6845(75) | 0.6833(69) | 0.6836(69) |
| Age | 13.797(23) | 13.800(23) | 13.799(23) | 13.802(22) | 13.801(22) |
| H_0 | 67.36(54) | 67.32(55) | 67.34(55) | 67.26(50) | 67.28(50) |
| $100\theta_\chi$ | 1.04092(31) | 1.04185(29) | 1.04185(29) | 1.04184(29) | 1.04184(29) |
| σ_8 | 0.8111(60) | 0.8108(60) | 0.8109(60) | 0.8100(44) | 0.8099(44) |
| S_8 | 0.832(13) | 0.832(13) | 0.832(13) | 0.832(13) | 0.832(13) |
| τ_{reio} | 0.0544(73) | 0.0543(75) | 0.0547(76) | 0.0526(15) | 0.0527⁺⁽¹⁴⁾₋₍₁₆₎ |
| z_{re} | 7.67(73) | 7.67(75) | 6.76(67) | 6.98 | 6.99 |
| ζ_{UV} | | | | 26.9^{+2.1}_{-2.5} | 27.0^{+2.1}_{-2.5} |

with CMB to infer cosmology while constraining and marginalizing over ζ_{UV} .

When considering only CMB data, we sample the typical 6 cosmological parameters (see shaded parameters in Table 1), sampling τ_{reio} and using bisection to obtain the reionization timeline. For tanh, the bisection varies z_{re} , while for Gompertz we fix β to the mean value (7.66, the complexity 1 expression from PySR) and vary α . Therefore, we do not use the SR mapping from physical parameters to reionization – Eqs. (4) and (5) or alternatively Eqs. (10) and (11).

In contrast, when astrophysical data is included, tanh samples over z_{re} instead

of τ_{reio} and an additional likelihood component is calculated in Cobaya. For Gompertz, we do not sample any reionization parameter. Instead, we use SRFull or SRHalf to map physical parameters to reionization timeline and include the astrophysical likelihood component. Perhaps unsurprisingly, tanh reionization does a poor job of fitting the astrophysical data, with a χ^2 larger than Gompertz's by an order of magnitude, hence we do not show the tanh + CMB + DW results in [Table 1](#).

There is an apparent discrepancy between the different models in θ_x , a proxy for the angular scale of the acoustic oscillations (θ_*). The difference is due to our use of $100\theta_s$, which corresponds to the peak scale parameter defined exactly as the ratio of the sound horizon divided by the angular diameter at decoupling, with decoupling time given by the maximum of the visibility function, i.e. the standard choice for CLASS. In contrast, the Planck collaboration reports $100\theta_{\text{MC}}$, which is given by Eq. (6) in ⁶⁵, and corresponds to the standard choice in CosmoMC ³¹. Unsurprisingly, different reionization scenarios give similar values of $100\theta_s$.

Although [Table 1](#) does not display an error in the midpoint of reionization for gomp + SRFull + CMB + DW nor gomp + SRHalf + CMB + DW models, it is important to note that an error does exist. Unfortunately, it cannot be automatically computed with Cobaya because SRFull and SRHalf models do not sample over reionization parameters. Therefore, z_{re} has no meaning in our Gompertz CLASS² for models that take advantage of the mapping between physical parameters and reionization timeline.

Remarkably, the inferred value of S_8 remains consistent across all reionization models, even when σ_8 and Ω_m show small variations between models. This trend suggests that different reionization models neither alleviate nor exacerbate the S_8 tension. While this observation holds for the Planck PR3 data and for CMB + DW, we anticipate that incorporating low-redshift Baryon Acoustic Oscillation (BAO) data may affect this conclusion. Future work will explore the implications of Gompertz reionization for the joint analysis of CMB and low-redshift data.

²This oversight can be corrected; however, it would require re-running the chains.

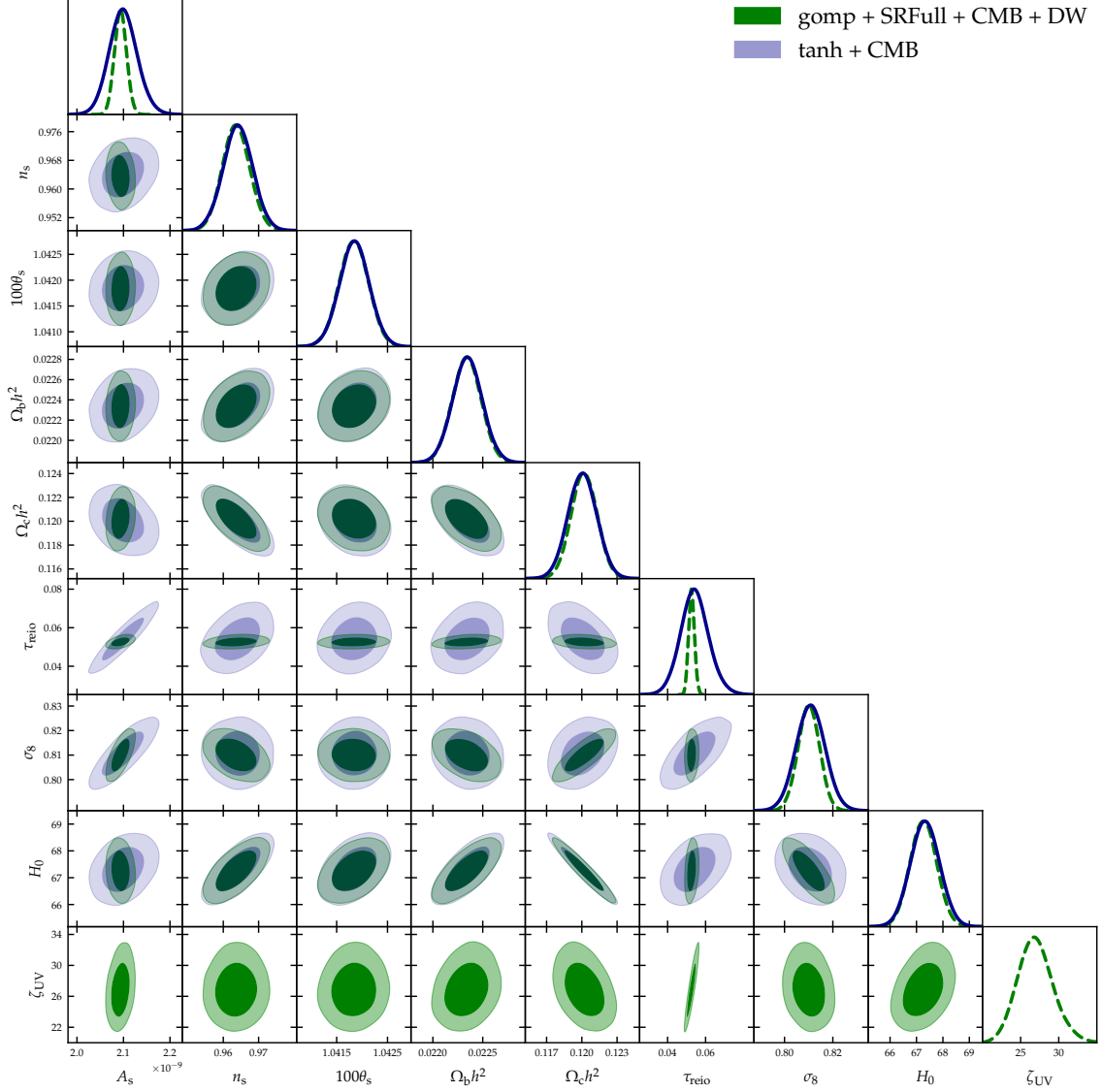


Figure 8: Analysis of CMB data and astrophysical data treating τ_{reio} as a derived parameter using Eqs. (1) to (5) vs. sampling it with the conventional tanh model. Here gomp + SRFull combines our Gompertz universal shape with the rescaling pivot and tilt obtained via symbolic regression. Note that for gomp + SRFull we do not sample over z_{re} , since Eq. (1) does not depend on it but we use the astrophysical data to constrain and marginalize over reionization astrophysics. The green (blue) contours correspond to the constraints obtained with our Gompertz universal shape (tanh model).

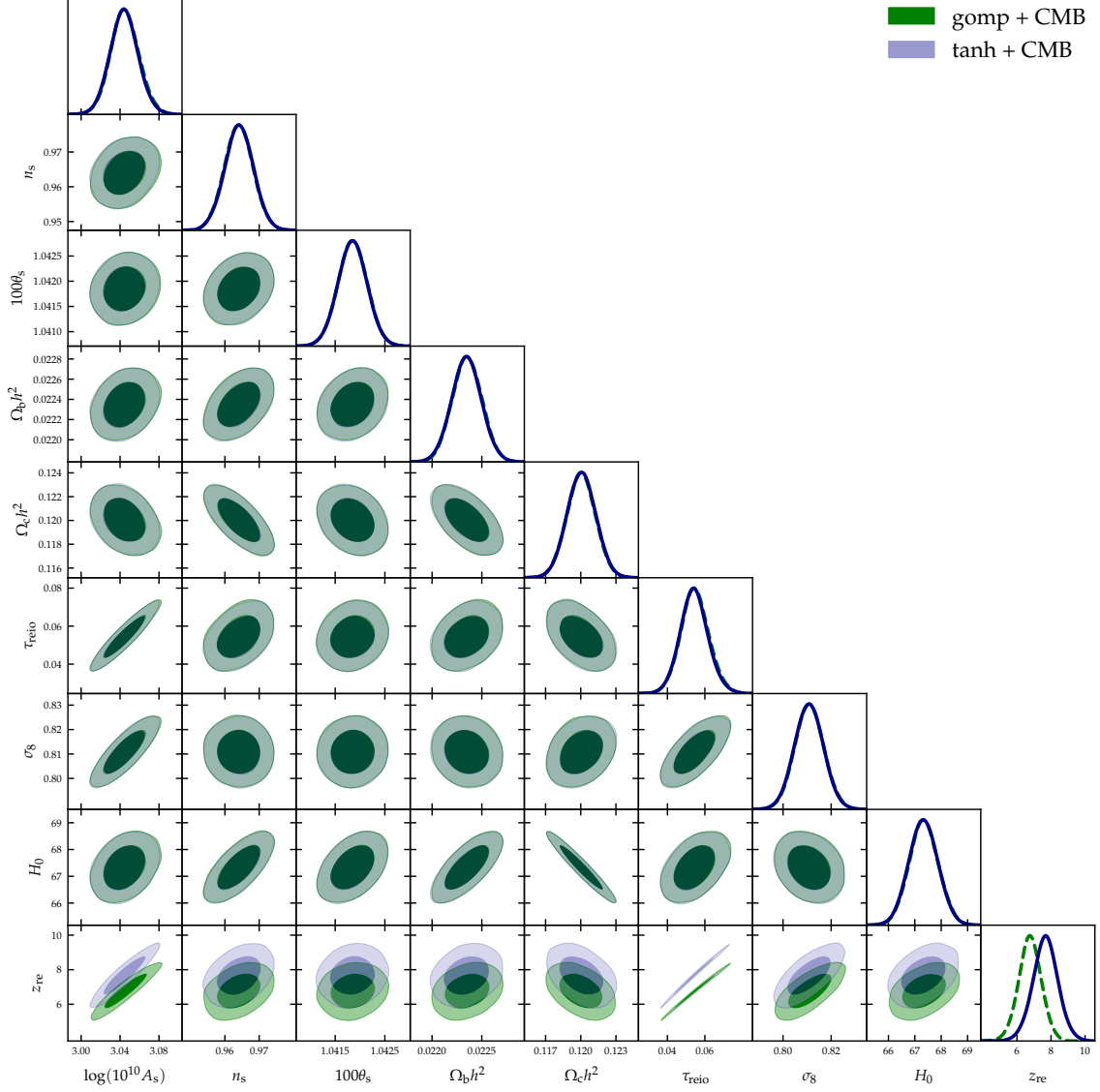


Figure 9: Validation of our universal shape for x_{HI} in Eqs. (1) and (2) vs. the conventional tanh model using CMB data with sampling over τ_{reio} . Note that we have not use our mapping from physical parameters to τ_{reio} . Here, we use the standard choice of sampling over optical depth and obtain the corresponding reionization history via bisection. The green (blue) contours correspond to the constraints obtained with our gomp (tanh) model.

Supplementary information No.

Acknowledgements This work is supported by The Major Key project of PCL. The authors acknowledge PCL's Cloud Brain for providing computational and data storage resources that have contributed to the results reported within this paper.

Declarations

Authors contributions P.M.C. and Y.L. contributed equally to all stages of the project. M.C. contributed to the implementation of the symbolic regression algorithm.

Correspondence and requests for materials Should be addressed to Paulo Montero-Camacho and Yin Li.

Code & data availability The paper source files and the scripts used in this work are available at github.com/eelregit/5par. The 21cmFAST simulation data and the MCMC chains are available upon reasonable requests from the correspondence authors.

Funding Not applicable.

Competing interests The authors declare no competing interests.

Ethics approval Not applicable.

Consent to participate Not applicable.

Consent for publication Not applicable.

References

- [1] Planck Collaboration, N. Aghanim, Y. Akrami, M. Ashdown, J. Aumont, C. Baccigalupi et al., *Planck 2018 results. VI. Cosmological parameters*, *Astron. Astrophys.* **641** (2020) A6 [1807.06209].
- [2] X. Jin, J. Yang, X. Fan, F. Wang, E. Bañados, F. Bian et al., *(Nearly) Model-independent Constraints on the Neutral Hydrogen Fraction in the Intergalactic Medium at z 5-7 Using Dark Pixel Fractions in Ly α and Ly β Forests*, *ApJ* **942** (2023) 59 [2211.12613].
- [3] J.P. Gardner, J.C. Mather, M. Clampin, R. Doyon, M.A. Greenhouse, H.B. Hammel et al., *The James Webb Space Telescope*, *Space Sci. Rev.* **123** (2006) 485 [astro-ph/0606175].
- [4] A.-C. Eilers, R.A. Simcoe, M. Yue, R. Mackenzie, J. Matthee, D. Ďurovčíková et al., *EIGER. III. JWST/NIRCam Observations of the Ultraluminous High-redshift Quasar J0100+2802*, *ApJ* **950** (2023) 68 [2211.16261].

- [5] N.J. Adams, C.J. Conselice, L. Ferreira, D. Austin, J.A.A. Trussler, I. Juodžbalis et al., *Discovery and properties of ultra-high redshift galaxies ($9 < z < 12$) in the JWST ERO SMACS 0723 Field*, *Mon. Not. Roy. Astron. Soc.* **518** (2023) 4755 [2207.11217].
- [6] L.D. Bradley, D. Coe, G. Brammer, L.J. Furtak, R.L. Larson, V. Kokorev et al., *High-redshift Galaxy Candidates at $z = 9-10$ as Revealed by JWST Observations of WHL0137-08*, *ApJ* **955** (2023) 13 [2210.01777].
- [7] C.T. Donnan, D.J. McLeod, J.S. Dunlop, R.J. McLure, A.C. Carnall, R. Begley et al., *The evolution of the galaxy UV luminosity function at redshifts $z \approx 8 - 15$ from deep JWST and ground-based near-infrared imaging*, *Mon. Not. Roy. Astron. Soc.* **518** (2023) 6011 [2207.12356].
- [8] Y. Ning, Z. Cai, X. Lin, Z.-Y. Zheng, X. Feng, M. Li et al., *Unveiling Luminous Ly α Emitters at $z \approx 6$ through JWST/NIRCam Imaging in the COSMOS Field*, *Astrophys. J. Let.* **963** (2024) L38 [2312.04841].
- [9] Planck Collaboration, N. Aghanim, Y. Akrami, F. Arroja, M. Ashdown, J. Aumont et al., *Planck 2018 results. I. Overview and the cosmological legacy of Planck*, *Astron. Astrophys.* **641** (2020) A1 [1807.06205].
- [10] U. Natale, L. Pagano, M. Lattanzi, M. Migliaccio, L.P. Colombo, A. Gruppuso et al., *A novel CMB polarization likelihood package for large angular scales built from combined WMAP and Planck LFI legacy maps*, *Astron. Astrophys.* **644** (2020) A32 [2005.05600].
- [11] S. Paradiso, L.P.L. Colombo, K.J. Andersen, R. Aurlien, R. Banerji, A. Basyrov et al., *BEYONDPLANCK. XII. Cosmological parameter constraints with end-to-end error propagation*, *Astron. Astrophys.* **675** (2023) A12 [2205.10104].
- [12] Y. Qin, V. Poulin, A. Mesinger, B. Greig, S. Murray and J. Park, *Reionization inference from the CMB optical depth and E-mode polarization power spectra*, *Mon. Not. Roy. Astron. Soc.* **499** (2020) 550 [2006.16828].
- [13] D. Paoletti, D.K. Hazra, F. Finelli and G.F. Smoot, *The asymmetry of dawn: evidence for asymmetric reionization histories from a joint analysis of cosmic microwave background and astrophysical data*, *arXiv e-prints* (2024) arXiv:2405.09506 [2405.09506].
- [14] W. Giarè, E. Di Valentino and A. Melchiorri, *Measuring the reionization optical depth without large-scale CMB polarization*, *arXiv e-prints* (2023) arXiv:2312.06482 [2312.06482].
- [15] L. Pagano, J.M. Delouis, S. Mottet, J.L. Puget and L. Vibert, *Reionization optical depth determination from Planck HFI data with ten percent accuracy*, *Astron. Astrophys.* **635** (2020) A99 [1908.09856].
- [16] C. Heinrich and W. Hu, *Reionization effective likelihood from Planck 2018 data*, *Physical Review D* **104** (2021) 063505.
- [17] M. Tristram, A.J. Banday, M. Douspis, X. Garrido, K.M. Górski, S. Henrot-Versillé et al., *Cosmological parameters derived from the final Planck data release (PR4)*, *Astron. Astrophys.* **682** (2024) A37 [2309.10034].
- [18] R. de Belsunce, S. Gratton, W. Coulton and G. Efstathiou, *Inference of the optical depth to reionization from low multipole temperature and polarization Planck data*, *Mon. Not. Roy. Astron. Soc.* **507** (2021) 1072 [2103.14378].
- [19] P. Montero-Camacho and Y. Mao, *Extracting the astrophysics of reionization from the Ly α forest power spectrum: a first forecast*, *Mon. Not. Roy. Astron. Soc.* **508** (2021) 1262 [2106.14492].
- [20] The HERA Collaboration, Z. Abdurashidova, T. Adams, J.E. Aguirre, P. Alexander, Z.S. Ali et al., *Improved Constraints on the 21 cm EoR Power Spectrum and the X-Ray*

- Heating of the IGM with HERA Phase I Observations*, *arXiv e-prints* (2022) [arXiv:2210.04912](https://arxiv.org/abs/2210.04912) [[2210.04912](https://arxiv.org/abs/2210.04912)].
- [21] N.Y. Gnedin and P. Madau, *Modeling cosmic reionization*, *Living Reviews in Computational Astrophysics* **8** (2022) 3 [[2208.02260](https://arxiv.org/abs/2208.02260)].
- [22] R. Kannan, E. Garaldi, A. Smith, R. Pakmor, V. Springel, M. Vogelsberger et al., *Introducing the THESAN project: radiation-magnetohydrodynamic simulations of the epoch of reionization*, *Mon. Not. Roy. Astron. Soc.* **511** (2022) 4005 [[2110.00584](https://arxiv.org/abs/2110.00584)].
- [23] S. Murray, B. Greig, A. Mesinger, J. Muñoz, Y. Qin, J. Park et al., *21cmFAST v3: A Python-integrated C code for generating 3D realizations of the cosmic 21cm signal.*, *The Journal of Open Source Software* **5** (2020) 2582 [[2010.15121](https://arxiv.org/abs/2010.15121)].
- [24] X. Fan, E. Bañados and R.A. Simcoe, *Quasars and the Intergalactic Medium at Cosmic Dawn*, *Annual Review of Astron and Astrophys* **61** (2023) 373 [[2212.06907](https://arxiv.org/abs/2212.06907)].
- [25] M. Cranmer, *Interpretable Machine Learning for Science with PySR and SymbolicRegression.jl*, *arXiv e-prints* (2023) [arXiv:2305.01582](https://arxiv.org/abs/2305.01582) [[2305.01582](https://arxiv.org/abs/2305.01582)].
- [26] H. Trac, *Parametrizing the Reionization History with the Redshift Midpoint, Duration, and Asymmetry*, *Astrophys. J. Let.* **858** (2018) L11 [[1804.00672](https://arxiv.org/abs/1804.00672)].
- [27] H. Trac, N. Chen, I. Holst, M.A. Alvarez and R. Cen, *AMBER: A Semi-numerical Abundance Matching Box for the Epoch of Reionization*, *ApJ* **927** (2022) 186 [[2109.10375](https://arxiv.org/abs/2109.10375)].
- [28] A. Mesinger, S. Furlanetto and R. Cen, *21cmFAST: A fast, semi-numerical simulation of the high-redshift 21-cm signal*, *Monthly Notices of the Royal Astronomical Society* **411** (2011) 955 [[1003.3878](https://arxiv.org/abs/1003.3878)].
- [29] D. Blas, J. Lesgourgues and T. Tram, *The Cosmic Linear Anisotropy Solving System (CLASS) II: Approximation schemes*, *JCAP* **1107** (2011) 034 [[1104.2933](https://arxiv.org/abs/1104.2933)].
- [30] J. Torrado and A. Lewis, *Cobaya: Code for Bayesian Analysis of hierarchical physical models*, *JCAP* **05** (2021) 057 [[2005.05290](https://arxiv.org/abs/2005.05290)].
- [31] A. Lewis and S. Bridle, *Cosmological parameters from CMB and other data: A Monte Carlo approach*, *Phys. Rev. D* **66** (2002) 103511 [[astro-ph/0205436](https://arxiv.org/abs/hep-ph/0205436)].
- [32] A. Lewis, *Efficient sampling of fast and slow cosmological parameters*, *Phys. Rev. D* **87** (2013) 103529 [[1304.4473](https://arxiv.org/abs/1304.4473)].
- [33] Planck Collaboration, N. Aghanim, Y. Akrami, M. Ashdown, J. Aumont, C. Baccigalupi et al., *Planck 2018 results. V. CMB power spectra and likelihoods*, *Astron. Astrophys.* **641** (2020) A5 [[1907.12875](https://arxiv.org/abs/1907.12875)].
- [34] Planck Collaboration, N. Aghanim, Y. Akrami, M. Ashdown, J. Aumont, C. Baccigalupi et al., *Planck 2018 results. VIII. Gravitational lensing*, *Astron. Astrophys.* **641** (2020) A8 [[1807.06210](https://arxiv.org/abs/1807.06210)].
- [35] A. Lewis, *Cosmological parameters from WMAP 5-year temperature maps*, *Phys. Rev. D* **78** (2008) 023002 [[0804.3865](https://arxiv.org/abs/0804.3865)].
- [36] A. Doussot, H. Trac and R. Cen, *SCORCH. II. Radiation-hydrodynamic Simulations of Reionization with Varying Radiation Escape Fractions*, *ApJ* **870** (2019) 18 [[1712.04464](https://arxiv.org/abs/1712.04464)].
- [37] B. Gompertz, *Xxiv. on the nature of the function expressive of the law of human mortality, and on a new mode of determining the value of life contingencies. in a letter to francis baily, esq. frs &c*, *Philosophical transactions of the Royal Society of London* (1825) 513.
- [38] A. Gelman and D.B. Rubin, *Inference from Iterative Simulation Using Multiple Sequences*, *Statistical Science* **7** (1992) 457.
- [39] L.C. Keating, L.H. Weinberger, G. Kulkarni, M.G. Haehnelt, J. Chardin and

- D. Aubert, *Long troughs in the Lyman- α forest below redshift 6 due to islands of neutral hydrogen*, *Mon. Not. Roy. Astron. Soc.* **491** (2020) 1736 [[1905.12640](#)].
- [40] B. Greig and A. Mesinger, *The global history of reionization*, *Mon. Not. Roy. Astron. Soc.* **465** (2017) 4838 [[1605.05374](#)].
- [41] C. Cain, A. D’Aloisio, N. Gangolli and G.D. Becker, *A Short Mean Free Path at $z = 6$ Favors Late and Rapid Reionization by Faint Galaxies*, *Astrophys. J. Let.* **917** (2021) L37 [[2105.10511](#)].
- [42] S. Anselmi, M.F. Carney, J.T. Giblin, S. Kumar, J.B. Mertens, M. O’Dwyer et al., *What is flat Λ CDM, and may we choose it?*, *JCAP* **2023** (2023) 049 [[2207.06547](#)].
- [43] J. Flitter and E.D. Kovetz, *New tool for 21-cm cosmology. I. Probing Λ CDM and beyond*, *Phys. Rev. D* **109** (2024) 043512 [[2309.03942](#)].
- [44] I.M. Sobol’, *On the distribution of points in a cube and the approximate evaluation of integrals*, *Zhurnal Vychislitel’noi Matematiki i Matematicheskoi Fiziki* **7** (1967) 784.
- [45] A.B. Owen, *Scrambling sobol’ and niederreiter–xing points*, *Journal of complexity* **14** (1998) 466.
- [46] J. Park, A. Mesinger, B. Greig and N. Gillet, *Inferring the astrophysics of reionization and cosmic dawn from galaxy luminosity functions and the 21-cm signal*, *Mon. Not. Roy. Astron. Soc.* **484** (2019) 933 [[1809.08995](#)].
- [47] H. Trac and R. Cen, *Radiative Transfer Simulations of Cosmic Reionization. I. Methodology and Initial Results*, *ApJ* **671** (2007) 1 [[astro-ph/0612406](#)].
- [48] A. Liu, J.R. Pritchard, R. Allison, A.R. Parsons, U. Seljak and B.D. Sherwin, *Eliminating the optical depth nuisance from the CMB with 21 cm cosmology*, *Phys. Rev. D* **93** (2016) 043013 [[1509.08463](#)].
- [49] S.C. Hotinli, *Cosmological probes of helium reionization*, *Phys. Rev. D* **108** (2023) 043528 [[2212.08004](#)].
- [50] P. Upton Sanderbeck and S. Bird, *Inhomogeneous He II reionization in hydrodynamic simulations*, *Mon. Not. Roy. Astron. Soc.* **496** (2020) 4372 [[2002.05733](#)].
- [51] J. Song, Q. Lu, B. Tian, J. Zhang, J. Luo and Z. Wang, *Prove Symbolic Regression is NP-hard by Symbol Graph*, Apr., 2024. 10.48550/arXiv.2404.13820.
- [52] M. Virgolin and S.P. Pissis, *Symbolic Regression is NP-hard*, July, 2022. 10.48550/arXiv.2207.01018.
- [53] M. Cranmer, A. Sanchez-Gonzalez, P. Battaglia, R. Xu, K. Cranmer, D. Spergel et al., *Discovering Symbolic Models from Deep Learning with Inductive Biases*, *arXiv e-prints* (2020) [arXiv:2006.11287](#) [[2006.11287](#)].
- [54] P. Montero-Camacho, Y. Zhang and Y. Mao, *The long-lasting effect of X-ray pre-heating in the post-reionization intergalactic medium*, *Mon. Not. Roy. Astron. Soc.* **529** (2024) 3666 [[2307.10598](#)].
- [55] A. Mesinger, A. Aykutalp, E. Vanzella, L. Pentericci, A. Ferrara and M. Dijkstra, *Can the intergalactic medium cause a rapid drop in Ly α emission at $z > 6$?*, *Mon. Not. Roy. Astron. Soc.* **446** (2015) 566 [[1406.6373](#)].
- [56] E. Sobacchi and A. Mesinger, *The clustering of Lyman α emitters at $z \approx 7$: implications for reionization and host halo masses*, *Mon. Not. Roy. Astron. Soc.* **453** (2015) 1843 [[1505.02787](#)].
- [57] C.A. Mason, T. Treu, M. Dijkstra, A. Mesinger, M. Trenti, L. Pentericci et al., *The Universe Is Reionizing at $z \sim 7$: Bayesian Inference of the IGM Neutral Fraction Using Ly α Emission from Galaxies*, *ApJ* **856** (2018) 2 [[1709.05356](#)].

- [58] C.A. Mason, A. Fontana, T. Treu, K.B. Schmidt, A. Hoag, L. Abramson et al., *Inferences on the timeline of reionization at $z \sim 8$ from the KMOS Lens-Amplified Spectroscopic Survey*, *Mon. Not. Roy. Astron. Soc.* **485** (2019) 3947 [[1901.11045](#)].
- [59] A. Hoag, M. Bradač, K. Huang, C. Mason, T. Treu, K.B. Schmidt et al., *Constraining the Neutral Fraction of Hydrogen in the IGM at Redshift 7.5*, *ApJ* **878** (2019) 12 [[1901.09001](#)].
- [60] B. Greig, A. Mesinger, F.B. Davies, F. Wang, J. Yang and J.F. Hennawi, *IGM damping wing constraints on reionization from covariance reconstruction of two $z \gtrsim 7$ QSOs*, *Mon. Not. Roy. Astron. Soc.* **512** (2022) 5390 [[2112.04091](#)].
- [61] B. Greig, A. Mesinger, E. Bañados, G.D. Becker, S.E.I. Bosman, H. Chen et al., *IGM damping wing constraints on the tail end of reionization from the enlarged XQR-30 sample*, *Mon. Not. Roy. Astron. Soc.* **530** (2024) 3208 [[2404.12585](#)].
- [62] B. Spina, S.E.I. Bosman, F.B. Davies, P. Gaikwad and Y. Zhu, *Damping wings in the Lyman- α forest: a model-independent measurement of the neutral fraction at $5.4 < z < 6.1$* , *arXiv e-prints* (2024) arXiv:2405.12273 [[2405.12273](#)].
- [63] D. Ďurovčiková, A.-C. Eilers, H. Chen, S. Satyavolu, G. Kulkarni, R.A. Simcoe et al., *Chronicling the reionization history at $6 \lesssim z \lesssim 7$ with emergent quasar damping wings*, *arXiv e-prints* (2024) arXiv:2401.10328 [[2401.10328](#)].
- [64] A.M. Morales, C.A. Mason, S. Bruton, M. Gronke, F. Haardt and C. Scarlata, *The Evolution of the Lyman-alpha Luminosity Function during Reionization*, *ApJ* **919** (2021) 120 [[2101.01205](#)].
- [65] Planck Collaboration, P.A.R. Ade, N. Aghanim, C. Armitage-Caplan, M. Arnaud, M. Ashdown et al., *Planck 2013 results. XVI. Cosmological parameters*, *Astron. Astrophys.* **571** (2014) A16 [[1303.5076](#)].